ELSEVIER

Journal of Marine Systems 32 (2002) 199–218

JOURNAL OF MARINE SYSTEMS

www.elsevier.com/locate/jmarsys

Water mass formation in the Black Sea during 1991–1995

J.V. Staneva [a,*], E.V. Stanev [b,1]

[a] National Institute of Meteorology and Hydrology, Bulgarian Academy of Sciences, Tzarigadsko Shosse Blvd., 66, 1000 Sofia, Bulgaria
[b] Department of Meteorology and Geophysics, University of Sofia, 5, James Bourchier Street, 1126, Sofia, Bulgaria

Received 13 November 2000; accepted 13 August 2001

Abstract

The concepts of the formation of Cold Intermediate Water (CIW) in the Black Sea are revisited on the base of numerical simulations with modular ocean model (MOM) for the period July 1991–June 1995 and validated against the data from three basin-wide surveys carried out during the same period. The time of replenishment of Cold Intermediate Layer (CIL) estimated from simulations varies between 5 and 12 years. The regionalization of the rate of cold water mass formation demonstrates that the dynamical control is of utmost importance. The year-to-year variability of that rate could reach about the half of annual mean values, and the magnitude of the interannual signal of the temperature in the core of Cold Intermediate Layer is comparable with the magnitude of the seasonal one. That explains some of the problems with the earlier estimates of formation rates derived from the observation. It is not only the insufficient data coverage in the horizontal, which biased the estimates, but also the undersampling of the seasonal signal in time. Therefore the parallel analysis of model and survey data could give a more objective tool when estimating the temporal variability of water mass formation.

Keywords: Black Sea; Water mass formation; Heat/freshwater fluxes; Numerical modelling

1. Introduction

The formation of surface and deep water masses in the Black Sea is shaped by the freshwater balance. The dilution of surface layer due to river runoff tends to decrease sea surface salinity (~18 psu). The Bosphorus undercurrent, transporting Mediterranean water into the deep layers, tends to increase the deep water salinity (~22.3 psu). The large vertical salinity contrast results in strong stability of stratification and insolation between layers, thus, the signals from the sea surface reach only very shallow depth. This favors the formation of stagnant conditions in the Black Sea and presents the prerequisite for the formation of Cold Intermediate Layer (CIL). The latter is a perennial characteristic of the thermohaline stratification that dominates the vertical profiles of temperature. The CIL is usually observed between 40 and 150 m and traces the interface between surface and deep water masses. Its low boundary approximately coincides with the depths affected by the seasonal signal originating at the sea surface.

There is one important difference between the mechanisms of water mass formation in the Black Sea and the ocean. While an important amount of

* Corresponding author. Present affiliation: Alfred-Wegener-Institut for Polar and Marine Research, Klimasystem, Bussestrasse 24, 24111, D-27570 Bremerhaven, Germany. Fax: +49-441-79-83-404.

E-mail address: jstaneva@awi-bremerhaven.de (J.V. Staneva).

[1] Present affiliation: ICBM, University of Oldenburg, Postfach 2503, D-26111 Oldenburg, Germany.

0924-7963/02/$ - see front matter
PII: S0924-7963(02)00038-6

intermediate and deep water in the ocean is formed throughout the year (see Marshall et al., 1993), that process in the Black Sea occurs during a short period (January–March) and is strongly controlled by the characteristics of the seasonal atmospheric signal.

The vertical conveyor belt in the Black Sea is well traced by the salinity distribution having its sink and source in the Bosphorus surface- and under-current, correspondingly. However, neither the temperature distribution, nor the heat exchange in the straits show pronounced vertical overturning. It can be easily estimated that the export of surface and intermediate water from the Black Sea into the Marmara Sea and the import of warmer Mediterranean water by the undercurrent do not give a large contribution in the Black Sea heat exchange. If we roughly estimate the heat exchange in the Bosphorus Straits as $\rho C_p V(T_{MS}-T_{BS})$, where ρ=1.10^3 kg m^{-3} is the density of the water, C_p=1.005×10^3 J (kg K)$^{-1}$ is the heat capacity, T_{MS}=14 °C is the temperature of the Marmara Sea, T_{BS}=8 °C is that of the Cold Intermediate Water (CIW), and V=150 km^3 year^{-1} is the magnitude of the two-layer exchange, we obtain for the total heating ~4×10^{10} W, which normalized by the basin area (~400 km^2) gives ~0.1 W m^{-2}. However, the monthly mean values at sea surface reach ~−150 W m^{-2} in winter and ~100 W m^{-2} in summer (two orders of magnitude larger than the net heat flux), leading us to the conclusion that, unlike the salinity conveyor belt, the heat conveyor belt has its source and sink at the sea surface, rather than in the strait.

Number of studies have been devoted to the formation of CIW (e.g. Ovchinnikov and Popov, 1987; Oguz et al., 1993; Ivanov et al., 1997). The earlier works were mainly focused on the phenomenology of CIL (mostly on its quasistationary characteristics), as well as on its seasonality, but so far, there are no much quantitative estimates on its interannual variability. There are also some estimates on the rates of water mass formation based on the analysis of cold water content of the CIL (Ovchinnikov and Popov, 1987). However, there are no clear ideas about the ranges of variability of water mass formation in different years. The latter is one of the main objectives in the present paper, which first describes the numerical model and data used, followed by the intercomparison between simulations and observations. The paper ends with a discussion of the main results and conclusions.

2. Description of the numerical model and observation data

2.1. The numerical model

We use the modular ocean model (MOM) version of Bryan–Semtner–Cox model (Bryan, 1969; Pacanowski et al., 1991). The model set-up for the Black Sea is widely described in the works of Staneva and Stanev (1997) and Stanev and Staneva (2000). The model has horizontal resolution of 1/12° in latitude, 1/9° in longitude (almost square grid elements with grid intervals of ~9 km). The bottom topography is taken from the UNESCO bathymetric map and discretized with the model resolution (Fig. 1). To avoid possible artifacts associated with the amplification of basin waves over the horizontal abyssal, which can happen in MOM if the vertical resolution in the abyss is coarse, we increase the discretization there. We have 24 levels, the thickness of layers varies from 5 m in the surface, 20, 10 until 90 m, decreasing to 400 m in the deep homogeneous layers and increases again to 60 m in the deepestmost levels.

The atmospheric forcing is calculated using bulk parameterization and twice daily atmospheric analysis data for temperature, relative humidity and winds at sea surface produced in Hadley Center, United Kingdom Meteorological Office (UKMO). The monthly mean distribution of cloud cover is taken from Sorkina (1974). Knowing about numerous problems with the adequacy of cloud data in the atmospheric models (analyses) motivated us to more deeply analyze the data of UKMO and ECMWF meteorological analyses. Some problems in the climatology of that data in the area of Black Sea resulted in the decision to use the climatological values.

The sea surface salinity is relaxed to the monthly mean climatological data interpolated for the current model time. The salt balance in the model is closed at the Bosphorus Straits by continuously adding a positive salinity flux. The latter is calculated from the diagnosed water balance at the sea surface using a simple physical model for the dependence of water exchange in the Straits on the freshwater balance at sea surface (for more detailed description of that parameterization, see the works of Stanev et al., 1997; Staneva and Stanev, 1998). The parameterization is calibrated against observations (Unluata et al.,

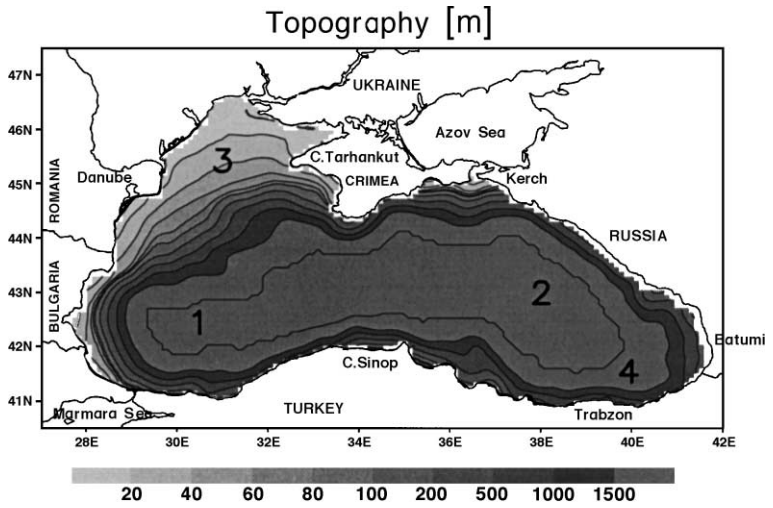

Fig. 1. The bottom topography. The following isolines are plotted: 10, 20, 40, 60, 80, 100, 200, 500, 1000, 1500 m.

1989) and simulations with a numerical model resolving hydraulic processes (Oguz et al., 1990). In order to simulate realistically the convection in the Bosphorus Straits area, a routine parameterizing the gravity plume and the resulting entrainment of the Black Sea water and detrainment of the plume water into the pycnocline is added to the main code. This parameterization suggests a virtual convective element, which entrains water from the ambient and increases its volume. This results in a decrease of the volume of the ambient water, which corresponds to an upward displacement of the water column. Thus, the plume penetrates deeper, increasing its volume and decreasing its density. These simple processes make the plume to behave as a mixing agent (Simeonov et al., 1997) rather than to only transport water downward. Details on the model sensitivity to different parameterizations are given by Stanev et al. (1997).

Mixing and diffusion in the horizontal are parameterized with biharmonic operators. The coefficients for momentum and tracers are: $A_h=K_h=0.1\times10^{19}$ cm^4 s^{-1}. The vertical mixing coefficient is $A_v=1.5$ cm^2 s^{-1}. The vertical diffusion in the model is parameterized as stability dependent and is calibrated against the independent data of Lewis and Landing (1991) based on the measurements of manganese and iron in the Black Sea:

$$K_v = aN^{-1},$$

where N is the Väisälä frequency, a=0.004 cm^2 s^{-2}. The bottom is insulating:

$$K_v(S,T)_z = 0,$$

where K_v is the coefficients of vertical diffusion. Details on the model sensitivity to different parameterizations are given by Stanev et al. (1997).

The circulation patterns are analyzed by Staneva and Stanev (1997) and Stanev and Staneva (2000). The final state of the simulations in these studies is used here as initial condition, and the model is further integrated with a forcing, which is based on the high-resolution data from atmospheric analyses.

2.2. Atmospheric data

The meteorological analysis data of UKMO have been used to generate the model forcing. These data include twice daily temperature, relative humidity and wind for the period June 1991–May 1995. Their resolution is 0.44° in latitude and longitude. In Fig. 2a–c, we show the temporal variability of area averaged UKMO data for the period of integration (the annual mean values for the individual years and the winter values — in brackets — are displayed below each graph).

The temporal variability of basin mean magnitude of wind stress and heat flux are shown in Fig. 2d and e, correspondingly. We remind here that wind stress

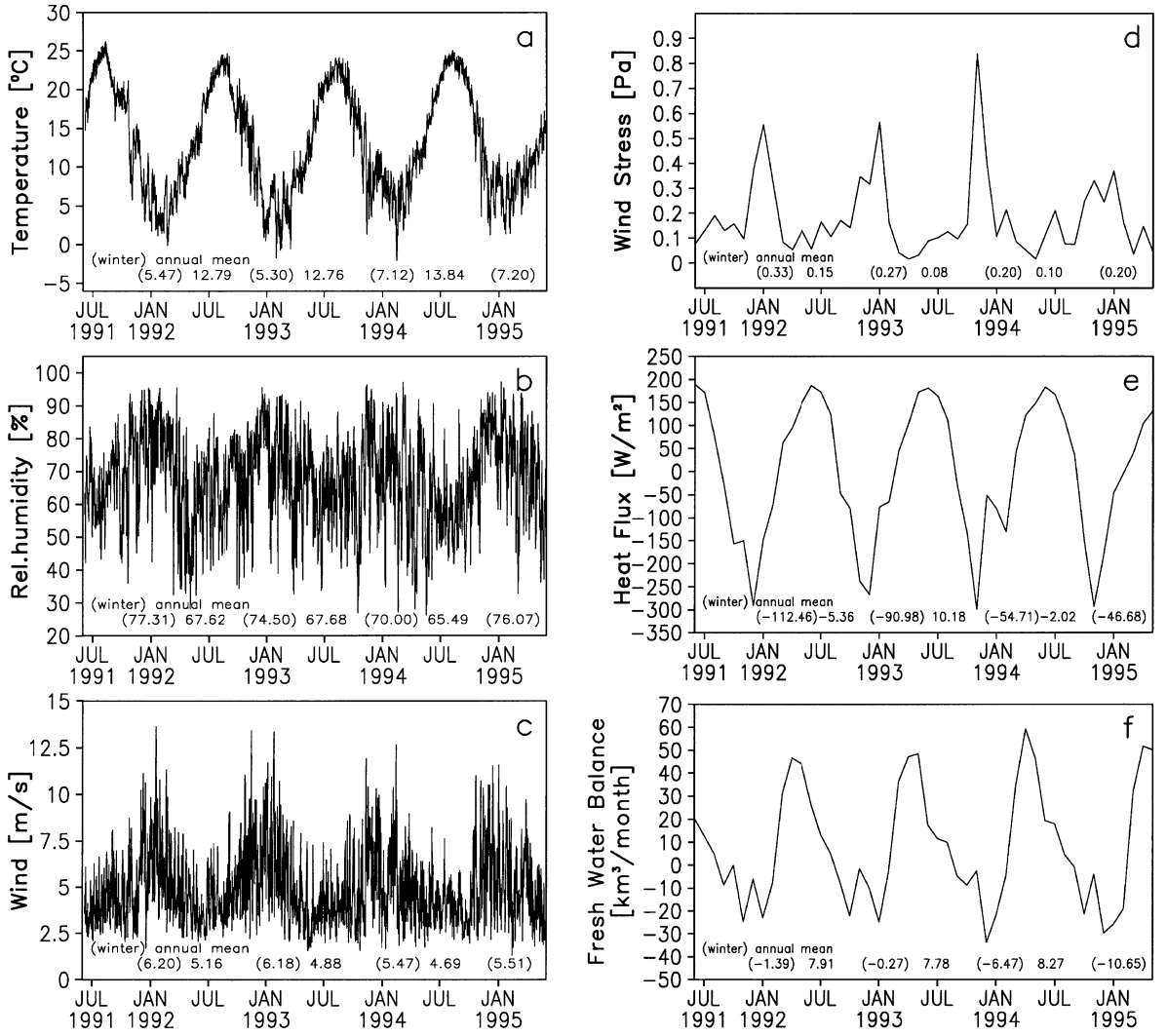

Fig. 2. Area averaged forcing data (a–c) and the corresponding monthly mean fluxes, diagnosed by the model as a function of time: (a) atmospheric temperature, (b) relative humidity, (c) wind magnitude, (d) wind stress, (e) heat flux, (f) freshwater flux. The units are given in *y*-axis of each pattern. The annual mean values for 1992, 1993 and 1994 are printed at the bottom of each graph. The winter mean values are shown in brackets.

and air–sea heat flux are computed in the model using bulk parameterization (accounting for stability of stratification—the difference between SST and air-temperature), as well as current atmosphere values and simulated sea surface temperature. Thus, the results shown in Fig. 2d–f are practically model diagnostic of air–sea fluxes. The variability of the salt flux, diagnosed by the model (the relaxation term in the salinity equation results in virtual salt flux at sea surface) is shown in Fig. 2f. The wind stress magnitude is maximal in December–February and minimal in April–May, and variability approximately follows the mean course of the wind variability. However, the variability of the diagnosed heat flux does not follow the one of the temperature (the strongest cooling occurs 1–2 months earlier than the lowest atmosphere temperature) demonstrating that the heat fluxes are strongly shaped by atmosphere winds. The seasonal

variability in the wind magnitude could contribute to an increase in the cyclonic circulation in winter and decrease in summer. Such behavior in the Black Sea circulation has been previously reported by Filippov (1965), Blatov et al. (1984), Golubeva (1984), Stanev (1990), etc. Though the seasonal variability is dominating in all patterns, a pronounced year-to-year variability is clearly seen on these graphs (compare the values given in the bottom of each plot). The wind stress magnitude is highest in winter 1992 and lowest in 1994 and 1995. As we will see below, these year-to-year changes affect strongly the rates of cold water mass formation in different years. The local values of net heat flux range from ~ -200 W m^{-2} in December–January to ~ 100 W m^{-2} in June–August (Fig. 2e).

The intercomparison between the climate constructed from UKMO meteorological analyses data and the widely used reanalysis based on ECMWF data (not shown here) demonstrated that there was a good agreement between both types of data. Our decision here to use the UKMO meteorological analyses is motivated by their *better spatial resolution*!

2.3. The oceanic data

The model results in the present paper are verified against climatic and survey data, as well as against data measured by the Advanced Very High Resolution Radiometer (AVHRR). We will give first a brief information about the observations behind these data. The climatic data set is based on more than 25 000 station data in the last 70 years. The computation of monthly mean temperature and salinity is addressed by Altman et al. (1987). To describe the synoptic features in the Black Sea circulation, we use fine resolution measurements of temperature and salinity obtained under the Co-operative Marine Science Black Sea (CoMSBlack) program (Oguz et al., 1993, 1994). The first quasi-synoptic survey, called HydroBlack '91, was accomplished during 2–29 September 1991 with the participation of five research vessels. The resolution of the field measurements was 1/3° in the meridional and zonal directions, and the station network, where the CTD data for temperature and salinity were measured, comprised of 307 stations. The second survey, CoMSBlack '92 (4–26 July 1992), provided the same kind of data for 394 stations with approximately the same horizontal resolution. The third survey was carried out from 2–14 April 1993 and the station network included 300 stations. After quality control, we interpolated the station data in regular grid with resolution 1/12° in the meridional and 1/9° in the zonal direction (this is the model resolution, see Section 2.1) at 35 levels. Since there are number of studies based on these recent data, we will not describe them here but refer to the existing papers (Oguz et al., 1993, 1994).

3. Cold water mass formation and comparisons between simulations and observations

3.1. The response of the upper ocean to air–sea heat exchange and the preconditioning of water mass formation

The formation of cold water is largely dependent on the thermal state of the upper layer, which shapes the air–sea heat exchange. We address below the adequacy of thermal forcing in the model by analyzing the correlation between simulations and observations, first showing in Fig. 3 the Sea Surface Temperature (SST) in January, 1993 based on model simulations (Fig. 3b) and obtained from infra-red (AVHRR) images (Fig. 3c). The corresponding atmospheric temperature from the UKMO data (Fig. 3a) is shown as well. The following conclusions can be made. (1) There is a close correlation between the horizontal patterns of simulated and satellite data. (2) The atmospheric data are smoother than the SST, which is due to their coarser resolution and the different length scales in both data types. (3) The warm tongues in the southern and eastern Black Sea are dynamically caused (this pattern is not as pronounced in the atmospheric temperature). The agreement between the course of winter temperatures simulated and obtained from the AVHRR data (see the inset in Fig. 3b, c) demonstrates that the model resolves well the extremely cold events in 1993 (compare with the characteristics of forcing shown in Fig. 2). This result is very important for the understanding of year-to-year variations in the water mass formation. The simulated SST is lower in the shelf area than the observed one, which perhaps is due to the insufficient amount of AVHRR observations in

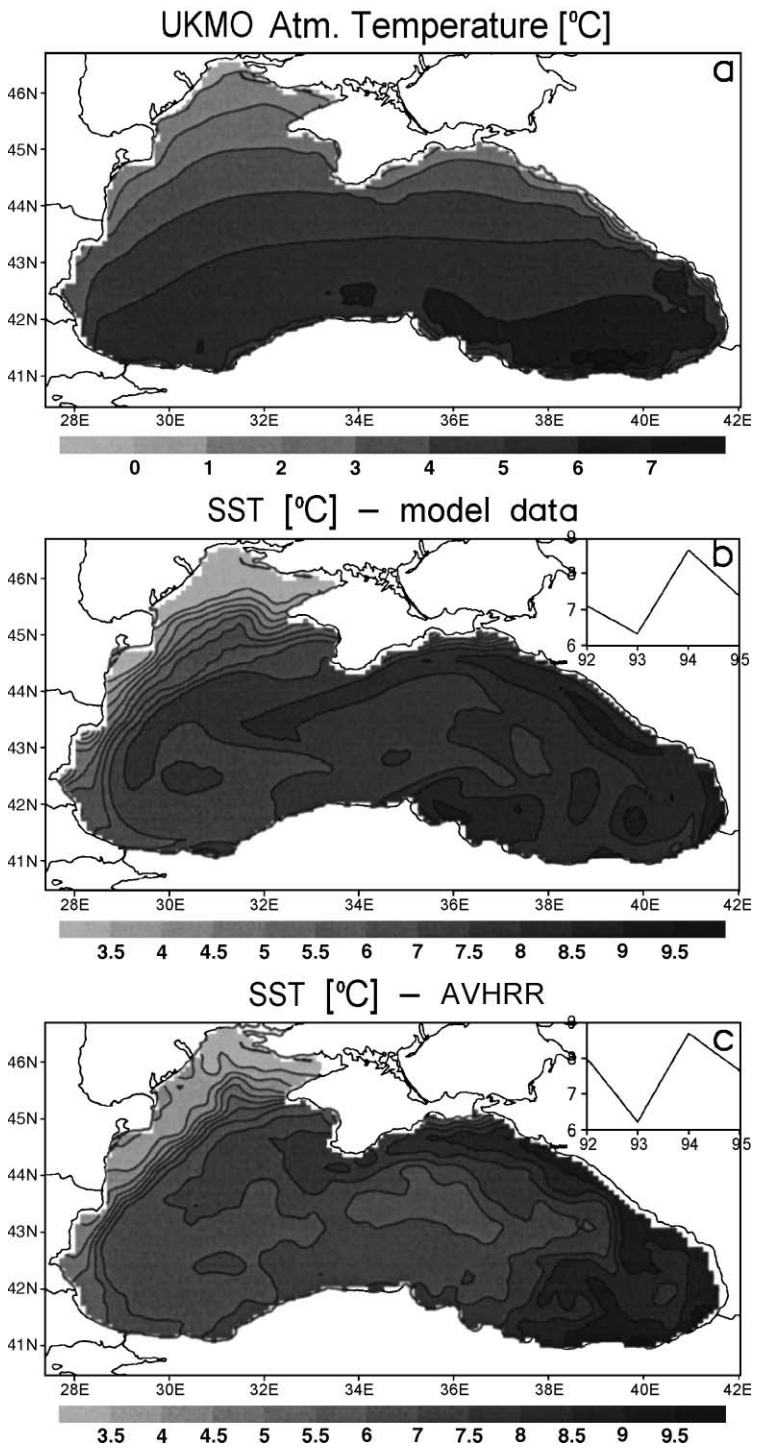

Fig. 3. Monthly mean temperatures [°C] in January 1993. (a) UKMO atmospheric temperature, (b) simulated SST, (c) SST from AVHRR data. The basin mean January temperatures during the period of integration are shown in the insets.

that area, making impossible to produce reliable averaging.

The vertical temperature cross-sections at 31.5°E in April 1993 demonstrates again quite satisfactory agreement between the simulations and observations (Fig. 4). The CoMSBlack survey data (measured shortly after the cooling period) reveal the penetration of cooled shelf water into the basin interior. The early phase of the formation of seasonal thermocline (see the warming of surface water in the southern part of the sea), the CIL and the doomed topography of the pycnocline is clearly identified by both observed and simulated patterns.

The position of the lower boundary of CIL (the depth, below which the temperature exceeds 8 °C) in September 1991 is used here for further validation of the model performance (Fig. 5). Not only the patterns are similar, but also the values, demonstrating that the model is well calibrated to the Black Sea conditions. Obviously, the close correlation between the vertical and horizontal sections demonstrates that the model replicates adequately the observed CIL. The main difference between the two types of data is the slightly wider extension of coastal anticyclones in the simulations. Probably, further downscaling of the model and use of less dissipative schemes (Staneva et al., 2001)

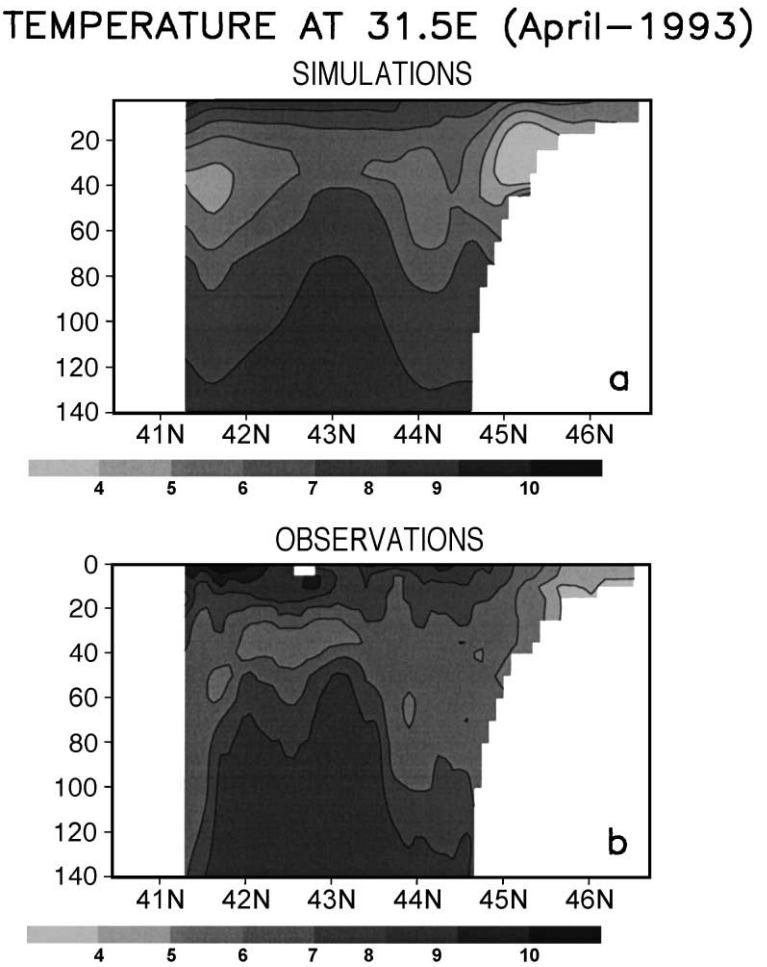

Fig. 4. Meridional cross-sections of temperature [°C] at 31.5°E in April 1993. (a) Simulated data, (b) survey data.

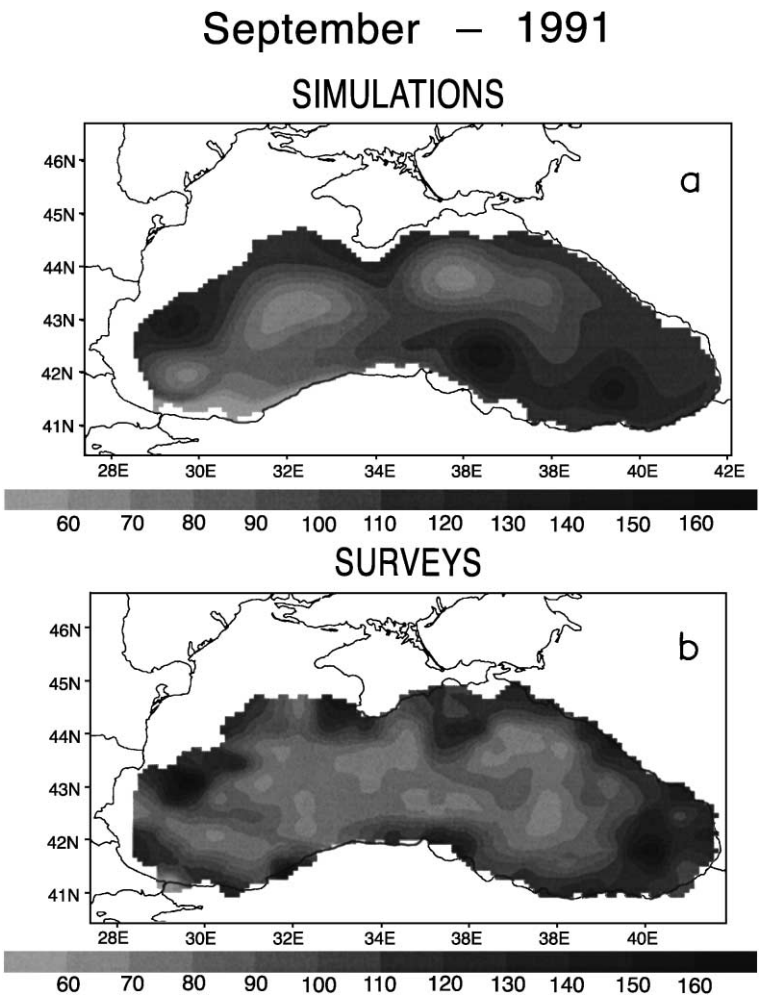

Fig. 5. Lower boundary of CIL [m] in September 1991. (a) From simulations, (b) from survey data.

is needed to more correctly simulate the small-scale patterns observed in the survey data.

3.2. Temporal variability of the water mass formation

The cold water mass formation reveals different behavior in regions characterized by different local conditions, which makes necessary to analyze separately this process in some locations (the positions are given in Fig. 1), which are representative for different conditions in the Black Sea (see also Staneva and Stanev, 1998). Locations 1 and 2 are in the western (C1) and eastern (C2) cyclonic areas, Location 4 is representative for the anticyclonic area in the eastern Black Sea (Batumi area) and Location 3 lies on the continental slope in the northwestern part (Shelf) with a depth of 140 m. The temporal variability of salinity and temperature profiles in the four locations is shown in Figs. 6 and 7, correspondingly. The surface layer (with low salinity values) is much thinner in C1 and C2 than in the Batumi region (compare Fig. 6a, b with Fig. 6d). This is associated with the general upwelling in the basin interior bringing deep saltier water close to the sea surface.

In all areas (cyclonic and anticyclonic), the salinity tends to decrease short after spring when the river runoff and precipitation reach their maxima. More detailed comparison of the variability in the cyclonic

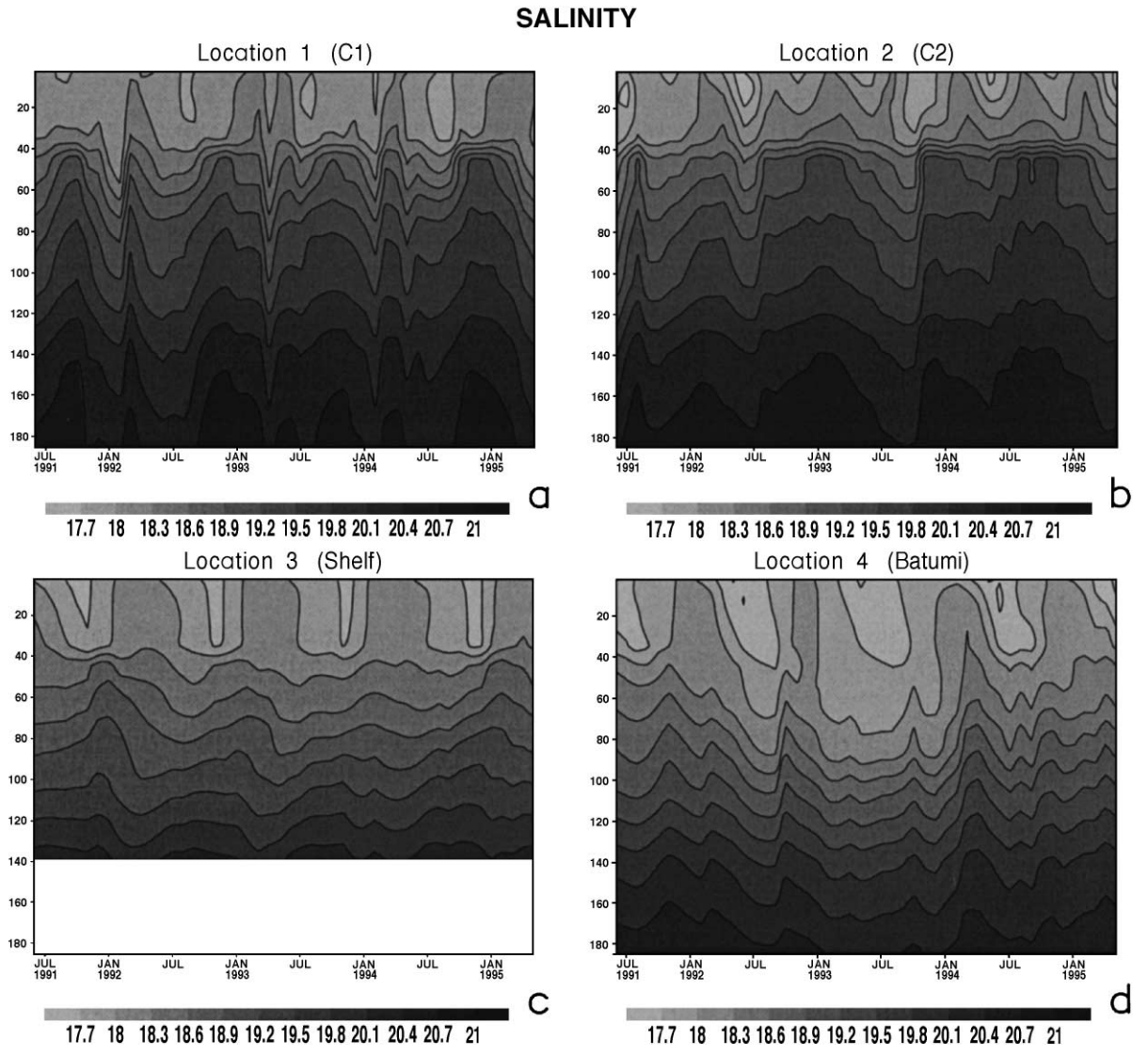

Fig. 6. Time versus depth plot of salinity [psu] in four locations. (a) Location 1: western cyclonic area (C1), 42.5°N, 32°E; (b) Location (2): eastern cyclonic area (C2) 43°N, 38.5°E; (c) Location 3: shelf area with a depth of 140 m, 44.5°N, 31°E; (d) Location 4, Batumi area, 41.5°N, 39.8°E. The locations 1–4 are plotted in Fig. 1.

and anticyclonic areas demonstrates that the decrease of salinity at ~40 m in spring–summer is delayed in the cyclonic area with several months in comparison with the coastal zone. This result is coherent with the concept that the basin interior gains fresh water from the coastal region and proves that the cross-frontal exchange needs some time (several months) to propagate the signal from coastal into the open sea area (see also Stanev et al., 2002).

The temporal variability simulated in the halocline is characterized with different periods and its appearance differs in the cyclonic and anticyclonic areas. The seasonal variations are better pronounced over the continental slope (Fig. 6c), whereas the oscillations in the basin interior do not reveal pronounced seasonality. This is consistent with the evidence that the seasonal intensification is well defined by the variations in the slope of halocline over the continental

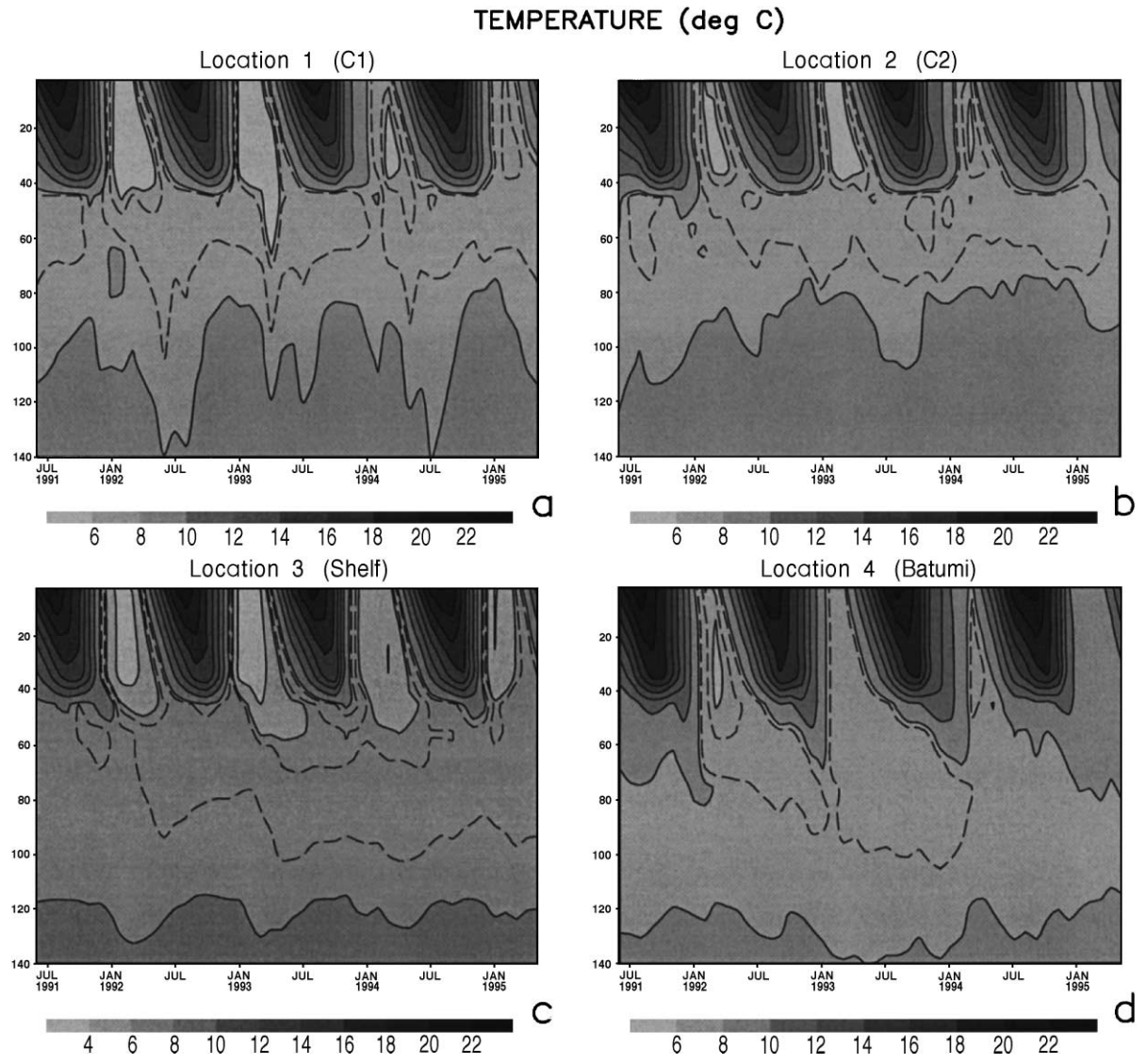

Fig. 7. Time versus depth plot of temperature [°C] in the same four locations as in Fig. 6. Dashed lines are used to have better resolution in the temperature lower than 8 °C.

slope (this is the case in Fig. 6c). No pronounced correlation exists between the variability in the area of Batumi eddy and that on the slope in the northwestern Black Sea, illustrating that the variations in the anticyclonic areas have quite different regional appearances.

The figure displaying the variability of temperature profiles (Fig. 7) is plotted for shallower depth interval than the salinity one since the temperature variations are almost negligible below the lower boundary of CIL. All patterns reveal typical seasonal variability, the outcropping is observed for a short period at the beginning of every year. The depth reached by convection is ~40 m in the cyclonic areas, while in the anticyclonic regions, it is about two times larger. On the other side, the winter temperature in the antycyclonic regions is higher than in the cyclonic ones. Similar behavior was previously reported by Staneva

and Stanev (1997), who demonstrated that the anticyclonic areas could dynamically enhance the penetration of CIW into the pycnocline. The more recent study by Stanev and Staneva (2001) shed more light in that process demonstrating that the rims of fronts and eddies present more effective dynamical agents controlling the ventilation of intermediate layer.

The lowest temperatures are simulated in the shelf, which is known as the main site of CIW formation (Kolesnikov, 1953). However, Ovchinnikov and Popov (1987) suggested later that the CIW was formed in the cyclonic eddies in basin interior. Obviously, according to the model simulations (see also Stanev and Staneva, 2001), both mechanisms of formation are not contradictory, but complementary!

The changing cooling in the individual years (smaller cooling in 1994 and 1995 and much larger in 1993–1994) is noteworthy when describing the forced response of CIL (Fig. 8). The slope of the contours of coldest water is vertical in the upper layer, and progresses with time at ~60–80 m (note that the temperature lower than 8 °C is plotted with dash lines) in all locations. From here, we can conclude that: (1) the CIL is periodically replenished with water from above, (2) the CIW tends to homogenize in the horizontal below the warm surface layer in summer–fall.

The thermohaline properties in the Back Sea tend to align to isopycnals, which is consistent with the concept that the diapycnal mixing is very small in the strongly stratified basin. We juxtapose below the seasonal variations of temperature profiles plotted against depth (Fig. 7) and the ones plotted in isopycnic coordinates (Fig. 8). The comparison between both types of representation of temporal variability makes possible to demonstrate more clearly the water mass formation process, including the outcropping and diapycnal intrusions. The outcropping starts in early fall, but the surface water reaches temperatures of CIW (lower than 8 °C) not earlier than January. The shape of isotherms at the beginning of the process of cold water mass formation (vertical or slopped isolines) demonstrates that mixing/convection propagates the cold signal in the range of 14.5–15.5 σ_t. This is well illustrated in C1 and C2 and proves that the cyclonic areas could be quite important for water mass formation, which is consistent with the ideas of Ovchinnikov and Popov (1987). The efficiency of this mechanism is enhanced by the cyclonic circulation, which preconditions the cooling of pycnocline. The basin-wide upwelling in the central locations displaces the pycnocline in winter near the sea surface, reducing thus the thickness of the thermal active layer. The wind mixing and convection (the latter is triggered by low temperatures in the thin surface layer) tend to mix the water column vertically. The intensification of the circulation in winter to spring season (caused by stronger wind forcing, see Fig. 2d) displaces the pycnocline towards its highestmost position and tends to increase the surface salinity. This process additionally intensifies water mass formation in the basin interior similarly to the well-known case of Gulf of Lions.

The diapycnal mixing is much weaker in the anticyclonic areas. The formation of CIW starts at 14–14.5 σ_t and affects much thinner σ_t layer. The homogeneous temperature (also salinity) on the deeper isopycnals reveals that the T–S characteristics remain almost unchanged by the seasonal signal below 15.5 σ_t that might be regarded as the lowest isopycnal depth reached by surface processes.

3.3. Year-to-year variation in the CIL

The above analysis of simulations could seem speculative if not compared with the data from the observations. Hopefully, the recent basin-wide surveys give such possibility and we will demonstrate in the remainder of the paper some intercomparisons. We remind here that we do not run the model in assimilation mode, thus, we can not anticipate a perfect correlation between observations and simulations. However, model statistics have to correlate with the one from the observations. Since the cold content and geometry of CIL are representative for the intermediate water mass formation, we will first analyze some statistical characteristics associated with the heat content (Fig. 9). The thickness of the CIL estimated from the simulations agrees quite well with the one estimated from the survey data and the deviations (the distance between the solid line and the triangles) are smaller than 1-rms variations that correspond to the horizontal variability derived from the observations.

We calculate the cold water content (Fig. 9b) as proportional to $\int(T_{i,j}-T_{8^\circ})dz$, where $T_{i,j}$ is the temperature of the CIL, $T_{8^\circ}=8^\circ$ and the integration is carried

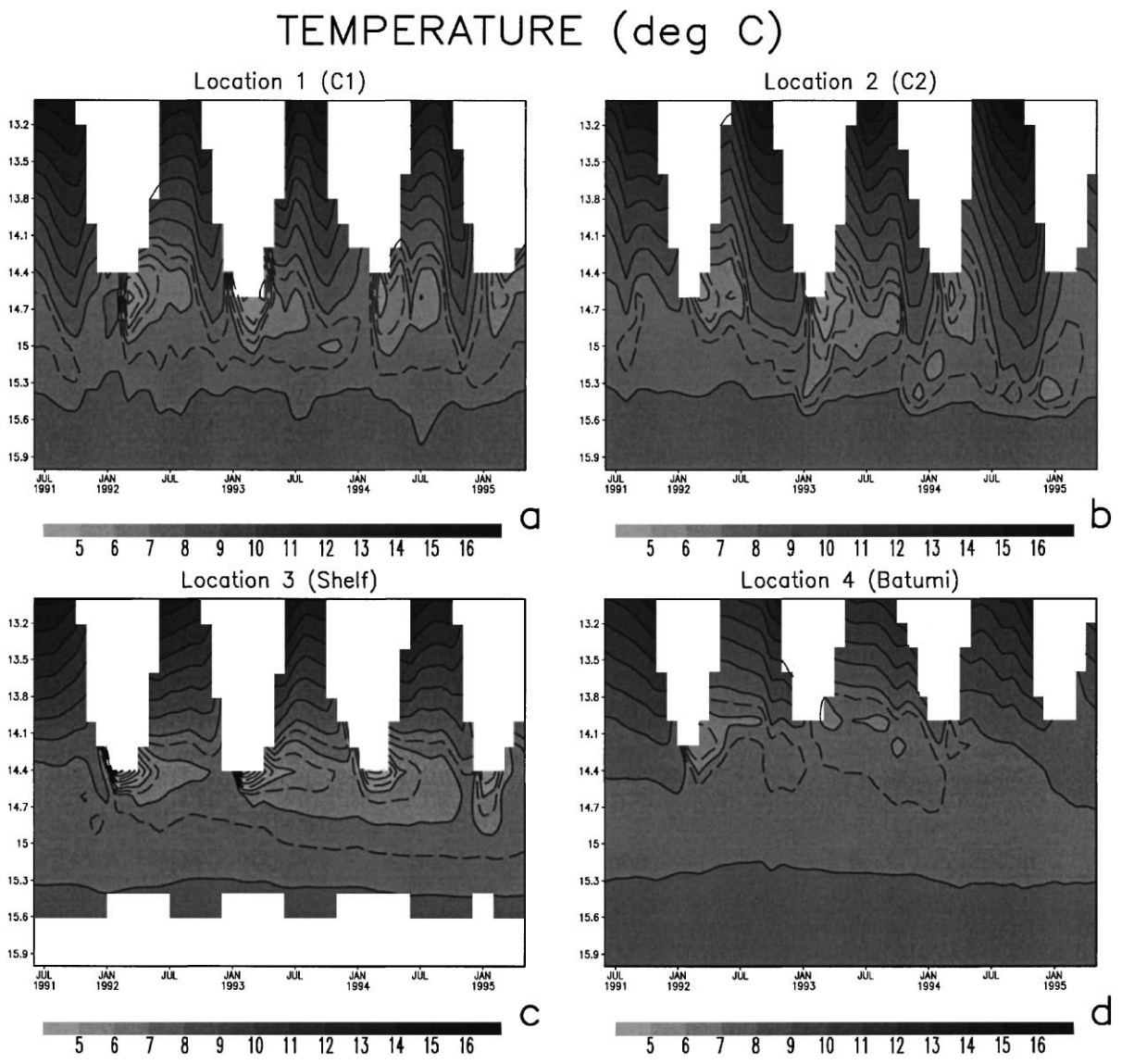

Fig. 8. Time versus σ_t plot of temperature [°C] in the same locations as in Fig. 6. Dashed lines are used to have better resolution in the temperature lower than 8 °C.

out between the upper and lower 8 °C isotherms (dz is the thickness of the model column). The corresponding estimates observed when using data from the observations are shown with triangles (their error bars are plotted as well). The conclusions from this plot can be summarized as follows. (1) The seasonal variability dominates the characteristics of CIL. (2) The thickness of the CIL and cold water content correlate well and both reach maxima in January–February. (3) The period of increase of CIL thickness and cold water content is about three times shorter than the period when they tend to decrease. This gives an approximate estimate that the mixing during the warmer part of the year is much less effective than in the cold part, which is mainly due to the increased stability (reduced mixing) in the seasonal thermocline (see Stanev, 1990). (4) The magnitude of the year-to-year variability is comparable with the one of seasonal signal. In the rela-

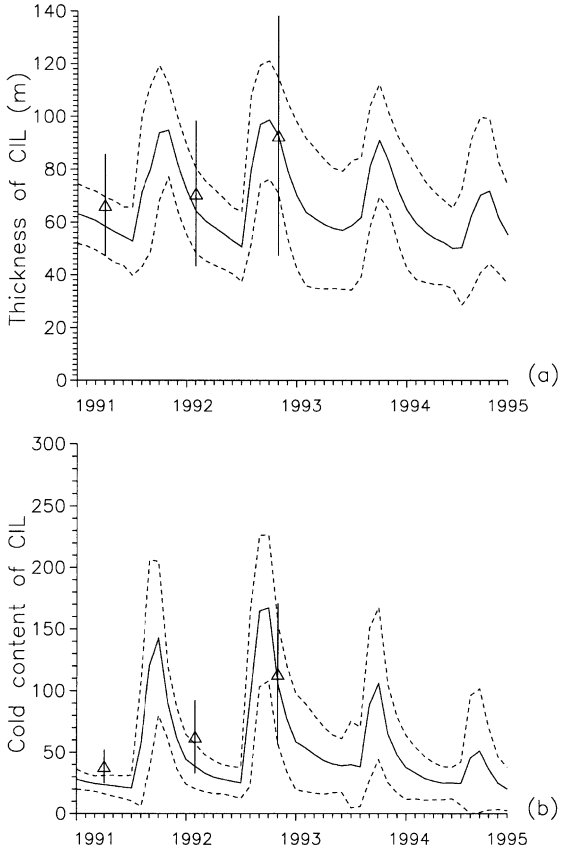

Fig. 9. The basin mean thickness of CIL (a) and cold water content. (b) The rms corresponding to the simulated horizontal variations of $\pm 1\sigma$ are plotted with dashed lines. The corresponding mean values from survey data are given with triangles. The vertical lines give the horizontal rms of $\pm 1\sigma$ estimated from the observations.

tively warmer years (1991 and 1995), the variations are much smaller and are better pronounced in the coastal area. (5) The agreement between simulations and observations is satisfactory giving some confidence to the estimates about the temporal variability of water mass formation discussed latter in this section. It is clear that using only survey data (even for 3 consecutive years 1991–1993) does not allow to make reliable estimates about the climatic changes and trends (as attempted in some studies). The high amplitude of the seasonal variations precludes correct conclusions if the data sampling does not well resolve the seasonal cycle (we remind that the surveys have not been carried out in the same time of year). Therefore, without considering the seasonal signal, the estimates could be seriously biased.

3.4. Regional characteristics of water mass formation

Number of studies are dealing with the rates of water mass formation based on the estimates of surface fluxes (Speer and Tzipermann, 1992; Lascaratos, 1993). The problem with these estimates is that the surface fluxes could warm or cool the ocean without contributing to intermediate or deep water formation. As clearly seen in Figs. 2 and 8, the cooling starts in fall, but the process of CIW formation does not start earlier than in December, when the temperatures reach values that are typical for the CIL. Not less important is that the waters formed at the sea surface can be classified as newly formed CIW only if they reach some specific isopycnic surface (larger than 14–14.5 σ_t depending on the area). Having in mind the above peculiarities, one can carry out simplified estimates on the formation rates, provided that profile data are available basin-wide (e.g. from climatic data). That is an interesting possibility, but one has to bear in mind that the discretization in time and space is quite insufficient for producing reliable quantification of the water mass formation. Also, the year-to-year variability (Fig. 9) might be quite strong, thus, climatic data (which do not well resolve individual months) are not always suitable when estimating the water mass formation rates. The numerical simulations can be used as a complement for contributing to more precise estimations.

From the analyses given above, it is evident that at least two conditions are necessary in the Black Sea that would make the water mass formation possible: (1) the temperature of cold water has to be below 8 °C and (2) the penetration of surface signal has to reach some particular depth (14.5 σ_t surface is accepted as the isopycnal layer below which the water is classified as belonging to the CIL). The analyses of simulated data demonstrate that the water mass formation starts later than the outcropping, and the delay associated with the time needed for the cooled water to sink down to 14.5 σ_t surface could reach several months (see, for example, Figs. 7 and 8). The surface cooling starting in fall "prepares" the water to reach the CIW, but the cold water mass formation does not always happen, particularly in some areas where the cooling

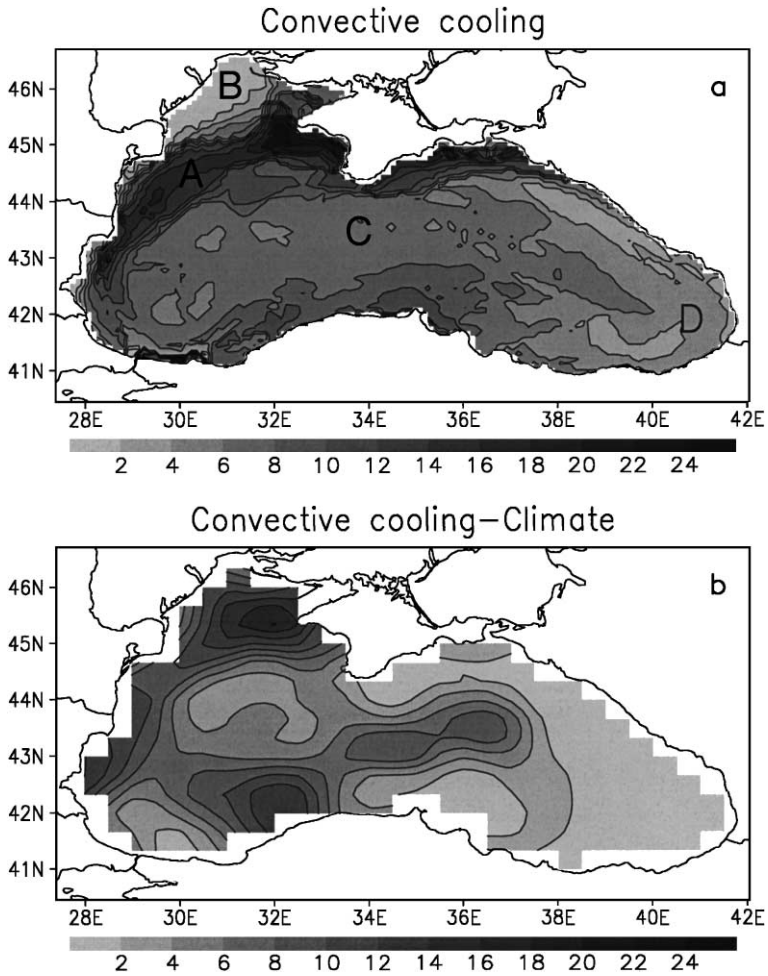

Fig. 10. Rates of water mass formation. The results are presented as thickness of water column [m] formed every year. (a) Water mass produced by convective cooling. (b) Estimates based on climatic data.

efficiency is small. Thus, to estimate the amount of water penetrating into the CIL, we compare the simulated "new" and "old" vertical temperature profiles at every time step and every grid point where the convection is active. If the cooling has reached deep enough isopycnal levels (e.g. σ_t=14.5 or deeper), then the difference in the heat content between 14.5 σ_t layer and the lower boundary of CIL at two consecutive time steps gives the rate of cooling. The latter normalized by the temperature gives a measure of the volume of newly formed CIW. If the convective cooling reaches the bottom and the bottom density is lower than 14.5, we estimate the water mass production as the difference between the heat content of the "new" and "old" water column normalized by the temperature. This means that the model diagnos-

Fig. 11. Atmospheric temperature (a), relative humidity (e) and wind magnitude (i) averaged over area A (shown in Fig. 10 and described in Section 3.3) as a function of time for the period of integration. Time variability of the difference between the atmospheric temperature of area A and areas B (b), C (c) and D (d). Time variability of the difference between the relative humidity of area A and areas B (f), C (g) and D (h). Time variability of the difference between the wind magnitude of area A and areas B (j), C (k) and D (h). The annual mean values for 1992, 1993 and 1994 are printed at the bottom of each graph. The winter mean values are shown in brackets.

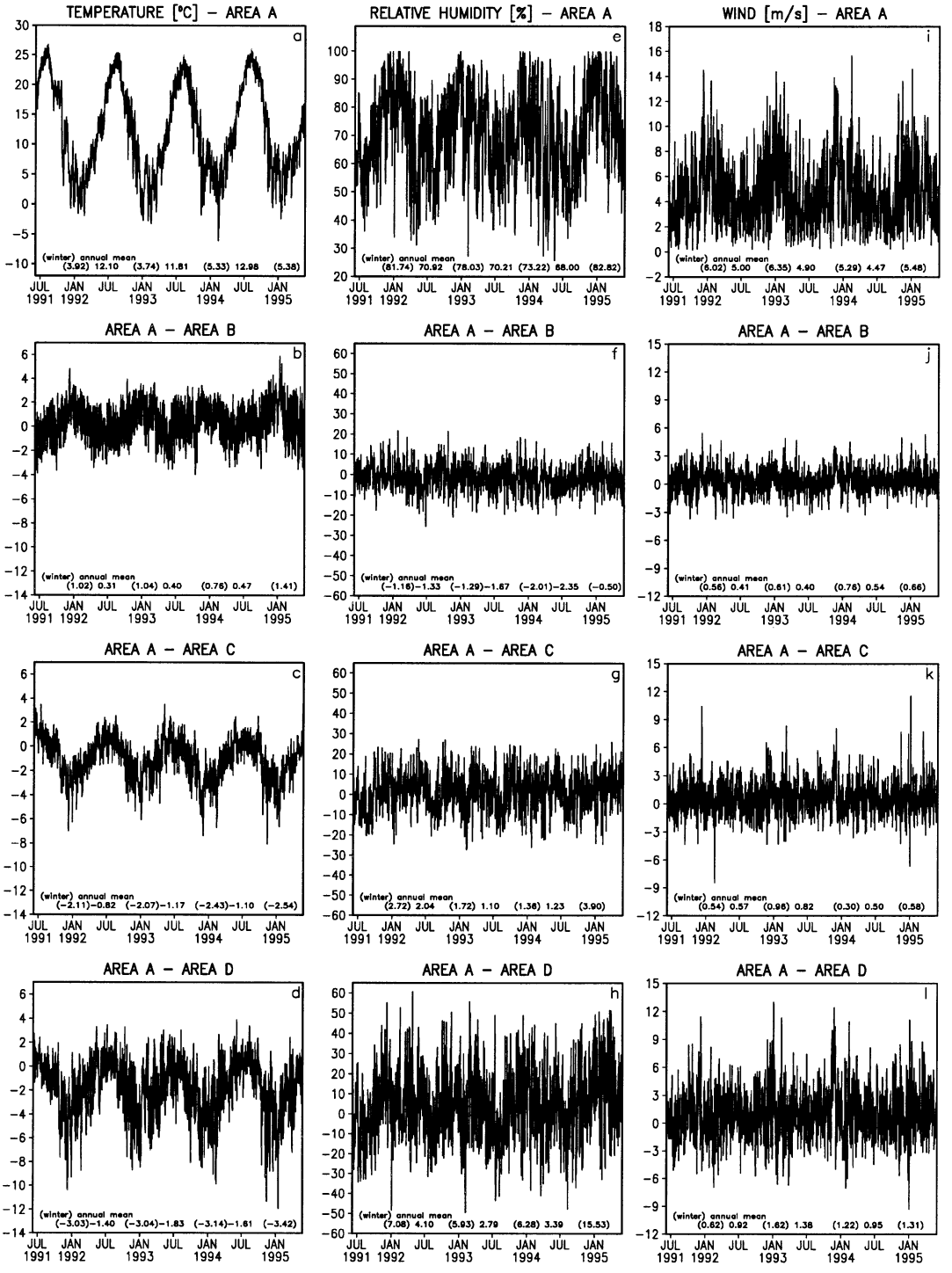
TEMPERATURE [°C] – AREA A
a
(winter) annual mean
(3.92) 12.10 (3.74) 11.81 (5.33) 12.98 (5.38)
RELATIVE HUMIDITY [%] – AREA A
e
(winter) annual mean
(81.74) 70.92 (78.03) 70.21 (73.22) 68.00 (82.82)
WIND [m/s] – AREA A
i
(winter) annual mean
(6.02) 5.00 (6.35) 4.90 (5.29) 4.47 (5.48)
AREA A – AREA B
b
(winter) annual mean
(1.02) 0.31 (1.04) 0.40 (0.76) 0.47 (1.41)
AREA A – AREA B
f
(winter) annual mean
(–1.16)–1.33 (–1.29)–1.67 (–2.01)–2.35 (–0.50)
AREA A – AREA B
j
(winter) annual mean
(0.56) 0.41 (0.61) 0.40 (0.76) 0.54 (0.66)
AREA A – AREA C
c
(winter) annual mean
(–2.11)–0.82 (–2.07)–1.17 (–2.43)–1.10 (–2.54)
AREA A – AREA C
g
(winter) annual mean
(2.72) 2.04 (1.72) 1.10 (1.36) 1.23 (3.90)
AREA A – AREA C
k
(winter) annual mean
(0.54) 0.57 (0.98) 0.82 (0.30) 0.50 (0.58)
AREA A – AREA D
d
(winter) annual mean
(–3.03)–1.40 (–3.04)–1.83 (–3.14)–1.61 (–3.42)
AREA A – AREA D
h
(winter) annual mean
(7.08) 4.10 (5.93) 2.79 (6.28) 3.39 (15.53)
AREA A – AREA D
l
(winter) annual mean
(0.62) 0.92 (1.62) 1.38 (1.22) 0.95 (1.31)
JUL JAN JUL JAN JUL JAN JUL JAN
1991 1992 1993 1994 1995

tics are not fully compatible in the deep ocean (where we estimate the rate of penetration of waters into the CIL) and on the shallow shelf (where we actually estimate the rate of the production of bottom water). This specification of the water mass formation rates focuses rather on the areas where the cooled water penetrates into the CIL from above, rather than on the amount of water originating from different source-areas that build the composition of CIW. In order to evaluate the origin and the contribution of the individual sources, age estimates would be more appropriate (see England, 1995).

The regional intensity of water mass formation measured as the water column penetrating annually the CIL is plotted in Fig. 10a as the mean for the whole period of integration. The most productive area is situated west of Crimea Peninsula, supporting some earlier findings based on the analysis of the depth of penetration of surface cooling (compare Fig. 10a with Fig. 2.29 from the study of Simonov and Altman, 1991). What has not been realized from the earlier studies is that the water mass formation was localized over a very narrow band along the shelf edge in the western Black Sea. The oversight of this important characteristic of water mass formation in the earlier studies could be due to the coarse resolution of climatic data in space and time that precluded resolving such features.

To demonstrate the problems of estimation of the water mass formation rates from climatic data, we carry out similar (but simplified) analysis as in the model simulations, comparing the evolution of the vertical profiles between every two months using monthly mean climatic data. The decrease of the heat content between σ_t=14.5 and the lower boundary of CIL is again taken as the measure of the cooling contributing to CIW formation. The patchy structure of the annually produced CIW (Fig. 10b) does not find hydrodynamical explanation. The local water mass formation area south of the Kerch Strait cannot be resolved from the coarse climatic data, as well, though there is other evidence from the observations that this area gives very important source of cold waters (Ivanov et al., 1997). However, in the main area of CIW formation that is to the west of Crimea Peninsula, the rates of newly formed water are comparable in the model estimates and in the ones based on climatic data.

The pattern in Fig. 10a makes possible to define several distinct areas of CIW penetration into intermediate depths: shelf edge region (A), that is the region where the effective thickness measuring the water mass penetration rate is more than 12 m y^{-1}; shallow shelf (B), that is the area between the northern boundary of region A and the cost; eastern region (D) where the intensity of the CIW penetration into the CIL is less than 6 m $year^{-1}$; and the remaining part of the Black Sea is the region (C). We remind here that the areas defined in that way and identify by the letters in Fig. 10 have nothing to do with the sampling locations given in Fig. 1. The temporal variability of the UKMO data—air temperature, relative humidity and wind plotted as the high frequency signal, as well as the model estimated monthly mean heat flux and wind stress magnitude averaged for area A, are shown in Figs. 11 and 12, correspondingly. To better illustrate the difference between the four areas, we plotted as well the difference between the signals in area A and the remaining areas.

Comparing the patterns of water mass formation rates and heat flux in the cooling season, we see that: (1) it is not the area of maximum water mass formation (West of Crimea, region A) where the total cooling is maximum. As seen in the comparison between Fig. 11a and b, the cooling on the shelf (area B) is by about 100 W m^{-2} smaller than the cooling at the shelf edge (area A). (2) The cooling south of Kerch Strait, which reaches the largest values basin-wide, does not result in as efficient water mass formation as in the western Black Sea. These results demonstrate that the local conditions/circulation govern the processes, thus, the dynamics shapes preponderantly the water mass formation. The inefficiency of cooling south of the Kerch Straits needs some explanations. Here, the diagnosed by the model heat flux in winter is very large, which is associated with the low

Fig. 12. The corresponding fluxes, diagnosed by the model as a function of time heat flux (a), and wind stress magnitude (e) averaged over area A (shown in Fig. 10 and described in Section 3.3) as a function of time for the period of integration. Time variability of the difference between heat flux of area A and areas B (b), C (c) and D (d). Time variability of the difference between wind stress magnitude of area A and areas B (f), C (g) and D (h). The annual mean values for 1992, 1993 and 1994 are printed at the bottom of each graph. The winter mean values are shown in brackets.

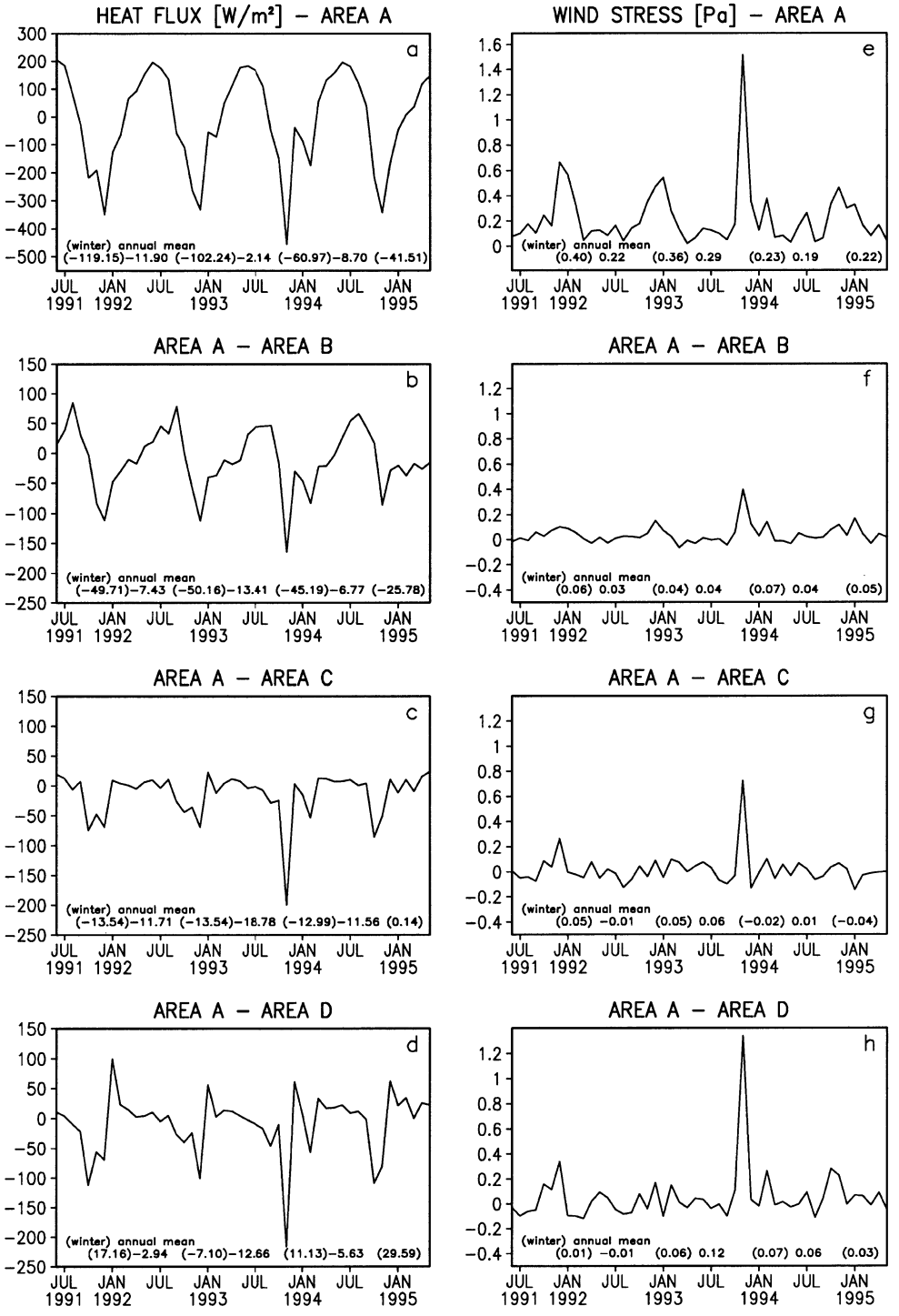
HEAT FLUX [W/m²] – AREA A
a
(winter) annual mean
(−119.15)−11.90 (−102.24)−2.14 (−60.97)−8.70 (−41.51)
WIND STRESS [Pa] – AREA A
e
(winter) annual mean
(0.40) 0.22 (0.36) 0.29 (0.23) 0.19 (0.22)
AREA A – AREA B
b
(winter) annual mean
(−49.71)−7.43 (−50.16)−13.41 (−45.19)−6.77 (−25.78)
AREA A – AREA B
f
(winter) annual mean
(0.06) 0.03 (0.04) 0.04 (0.07) 0.04 (0.05)
AREA A – AREA C
c
(winter) annual mean
(−13.54)−11.71 (−13.54)−18.78 (−12.99)−11.56 (0.14)
AREA A – AREA C
g
(winter) annual mean
(0.05) −0.01 (0.05) 0.06 (−0.02) 0.01 (−0.04)
AREA A – AREA D
d
(winter) annual mean
(17.16)−2.94 (−7.10)−12.66 (11.13)−5.63 (29.59)
AREA A – AREA D
h
(winter) annual mean
(0.01) −0.01 (0.06) 0.12 (0.07) 0.06 (0.03)
JUL JAN JUL JAN JUL JAN JUL JAN
1991 1992 1993 1994 1995

atmospheric temperature and relatively high SST, the latter is maintained in winter by the flow from the eastern (warm) basin. Under such conditions, the convection is not very deep since the cooled surface waters are mixed with the inflowing warm waters, therefore the local dynamics reduces the water mass formation rates. Just the opposite situation is observed in the western Back Sea, where the Rim Current transports cold waters originating from the shelf into a narrow area over the continental slope. The advective cooling of the water column in these areas preconditions the penetration of surface cooling down to the CIL.

The atmospheric temperature in the shelf region (area B) is minimal during the cold part of every year, which is illustrated by the positive anomalies in comparisons with area A (compare Fig. 11a and b). However, the net cooling is smaller than on the shelf edge and basin interior (Fig. 12b, c). The small efficiency of the northernmost shelf in the water mass formation reflects the fact that the low surface salinity and small depth of shelf reduce the heat capacity of water column, thus, the surface water reaches very low temperatures but only in a very thin diluted layer (Stanev, 1990). Even in the case when the cooling reaches the bottom, there is no penetration of surface water into the CIL from above, since the water density at the bottom in this area is below 14.5. This leads us to the conclusion that the area of the penetration of cooled water into the CIL needs to be beyond the shallow shelf zone since the water with T–S characteristics pertaining to the CIL are never simulated in the area of diluted shelf water.

The higher efficiency of cooling over the shelf edge (area A) is due to the mixing with open sea water, which increases salinity, and the density can reach values higher than $\sim$14.5, thus giving rise to water mass penetration into the CIL. More detailed analysis on the simulated data (including bottom temperature and salinity) showed that the highest efficiency of penetration of cooled water into the CIL is observed if the bottom is not much deeper than the depth of convection (which for the Black Sea conditions is between 40–70 m). In these areas, not only the density is appropriate for cold water penetration into the CIL, but also the temperature is sufficiently low. The latter is due to the continuous feeding of this zone by cold waters originating from the shelf. Beyond the shelf edge, that is in the area of coastal anticyclones, the thickness of upper layer (above the pycnocline) increases that would require stronger cooling to make the convection deep and water temperature low enough. This explains why beyond the depths 40–70 m, the amount of cold water penetrating into the CIL from above tends to decrease (Fig. 10a).

4. Discussion and conclusions

The fundamental question about to what extend the water mass formation could be regarded as local process is addressed below. Table 1 gives an idea about how active the cold water penetration into the CIL is in every region, specified in Section 3.4 during the different years of integration. Using the procedure described in the previous section, we estimate that the volume of the newly formed CIW averaged for 4-year period of integration is 4026 km^3 $year^{-1}$ (4919 km^3 in 1992, 5102 km^3 in 1994, 3591 km^3 in 1994 and 2492 km^3 in 1995). The mean volume of the CIL (between the 8° isotherms) for the same period is 22744 (minimum in 1995 of 18832 km^3 and maximum in 1993 of 24542 km^3). Thus, the time of replenishment of the CIW in our estimates taking into consideration the whole period of integration is $\sim$5.5 years. This value is consistent with the estimates by Ovchinnikov (1998) based on long-term survey data. More important in the context of the main subject in this paper is that the rates of formation show almost two-fold differences depending on atmospheric conditions in different winters (compare the values in 1993 and 1994).

The volume of the newly formed CIW in region A is 1702 km^3 $year^{-1}$, (during the cold 1993, it is maximal -2384 km^3 $year^{-1}$, while during the warmer 1994, it is about two times lower -1031 km^3 $year^{-1}$, indicating that 42.28% of the Black Sea cold water penetrates the CIL in the small area west of Crimea Peninsula. This ratio does not change significantly through the different years (it varies between 41.19% in 1995 and 43.28% in 1993). As proven by the analyses of our previous simulations (Stanev and Staneva, 2001) and observations (Simonov and Altman, 1991; Golubev and Kuftarkov, 1993), this is the region of extremely deep penetration of oceanic cooling.

Table 1
WM formation in the different years

	Black Sea	Region A	Region B	Region C	Region D
Surface ($\times 10^3$), km^2	4.12	0.53	0.34	2.40	0.85
Volume of the CIW, km^3	22 744	4530	1026	11 765	5423
Newly formed CIW, km^3	4026	1702	787	1145	392
for 1992	4683	1941	877	1436	429
for 1993	5520	2384	1059	1645	432
for 1994	3443	1452	700	923	368
for 1995	2458	1031	512	576	339

Although the winter basin minimum of surface temperature is observed in the northwestern shelf region (region B, see Figs. 3 and 11b), the amount of cold waters, which could be formed there is not significant (from 18.7% in 1992 to 20.8% in 1995 of the total amount). Obviously, the limited contribution of the shelf area in the water mass formation is due to relatively small rate of ventilation of the shelf region by open sea water (in the surface layer) and the compensatory export of bottom water into the open sea.

The outcropping in the basin interior (area C), associated with the intensification of cyclonic circulation in winter, is the major factor creating relatively large production there. The heat flux in area C is higher (less cooling) than that of the area A almost through the whole period of integration (only in spring both fluxes are compatible). This reflects the well-accepted concept that cooling of the Black Sea surface waters is more pronounced in coastal area, and warming is more pronounced in the basin interior. In the latter region, the compensatory cooling is due to the upwelled CIW. In 1995 when the formation of new waters is quite small (due to the warm winter conditions, see also Fig. 12c), this percentage is lowest for the whole period (23.4% new waters), while in the colder years, it has relatively higher contribution (30.7% in 1992). The contribution of the basin interior in the water mass formation estimated from the model simulations supports the hypothesis of Ovchinnikov and Popov (1987) for the formation of the CIW. However, unlike to these authors, we do not find any model evidence that the CIW formation occurs preponderantly in the basin interior.

The easternmost part of the Black Sea performs opposite to the basin interior. Here, the relative contribution in water mass formation is larger during warm winter conditions (13.8% in 1995) against that during cold winters (7.8% in 1993). The surface conditions in region D are warmest (atmosphere temperature is higher than 10 °C in comparisons with northwestern shelf area B, Fig. 11). The hypothesis of Blatov et al. (1984) that most of the eastern basin is filled with imported water is supported by the very low production there (only 9.73% of the CIW are formed in that region).

At the end of the paper, we refer again to Fig. 10, which gives a synthesis conclusion about the water mass formation and the conveyor belt in the Black Sea. The area of efficient cooling acts as a small (compared to the basin surface) "throat" where the model predicts maximum penetration of cooled water into the CIL. This source region could be considered as the main source of the heat conveyor belt. A small part of this conveyor belt is closed in the Straits of Bosphorus, where the CIW (entrained by the Mediterranean Sea water) loses cold (note the large gradients confined to the shelf edge between Bosphorus Strait and Saharia Canyon). However, the largest part of cold water diffuses into the surface and deep layers over the entire basin. Thus, we conclude that the heat conveyor is "autonomous" in a sense that it starts and ends on the Black Sea surface, and only a minor part closes in the Bosphorus strait.

Acknowledgements

Data from the CoMSBlack surveys have been prepared in the frame of NATO Black Sea project and made available through Black Sea Environment Internet Node (BSEIN). We acknowledge the help of UKMO for making meteorological analyses data available under the research contract with CEC EV5V-CT92 0121, supplementary agreement CIPD

CT93 0016. This work was supported by the CEC Contract EU Fifth Framework Programme — Energy, environment and sustainable development, Contract No. EVK1-CT-2000-00051: Nutrient Management in the Danube Basin and its Impact on the Black Sea (daNUbs).

References

Altman, E.N., Gertman, I.F., Golubeva, Z.A., 1987. Climatological fields of salinity and temperature in the Black Sea. Gidrometeoizdat, Leningrad, 240 pp. (In Russian).

Blatov, A.S., Bulgakov, N.P., Ivanov, V.A., Kosarev, A.N., Tujilkin, V.S., 1984. Variability of Hydrophysical Fields in the Black Sea Gidrometeoizdat, Leningrad, 240 pp. (In Russian).

Bryan, K., 1969. A numerical method for the study of the circulation of the World Ocean. J. Comput. Phys. 4, 347–378.

England, M.H., 1995. The age of water and the ventilation timescales in a global ocean model. J. Phys. Oceanogr. 25, 2756–2777.

Filippov, D.M., 1965. The cold intermediate layer in the Black Sea. Oceanology 5, 47–52.

Golubev, Yu.N., Kuftarkov, A.Yu., 1993. On the air–sea exchange over the Black Sea. Meteorol. Gidrol. 3, 92–97 (in Russian).

Golubeva, A., 1984. Variability of the Black Sea heat balance. Trudy GOIN 180, 21–32 (In Russian).

Ivanov, L.I., Besiktepe, S., Ozsoy, E., 1997. The Black Sea cold intermediate layer. In: Ozsoy, E., Mikaelyan, A. (Eds.), Sensitivity to Change: Black Sea, Baltic Sea and North Sea. NATO ASI Series, vol. 27. Kluwer Academic Publishing, Dordrecht, The Netherlands, pp. 253–264.

Kolesnikov, A., 1953. Seasonal course of temperature, stability and vertical turbulent heat exchange in the open part of the Black Sea. Tr. Mor. Gudrol. Inst. USSR AS 3, 3–13 (in Russian).

Lascaratos, A., 1993. Estimation of deep and intermediate water mass formation rates in the Mediterranean Sea. Deep-Sea Res., Part II 40, 1327–1332.

Lewis, B.L., Landing, W.N., 1991. Manganese and iron in the Black Sea. Deep-Sea Res. 38, S773–S805.

Marshall, J.C., Nurser, A.J.G., Williams, R.G., 1993. Inferring the subduction rate and period over the North Atlantic. J. Phys. Oceanogr. 23, 1315–1329.

Oguz, T., Özsoy, E., Latif, M.A., Sur, H.I., Unluata, U., 1990. Modeling of hydrographically controlled exchange flow in the Bosphorus Strait. J. Phys. Oceanogr. 20, 945–965.

Oguz, T., Besiktepe, S., Bastrurk, O., Salihoglu, I., Aubreym, D., Balci, A., Demirov, E., Diaconu, V., Dorogan, L., Duman, M., Ivanov, L., Konovalov, S., Stoyanov, A., Turgul, S., Vladimirov, V., Hilmaz, A., 1993. CoMSBlack '92A Physical and Chemical Intercalibration Workshop. IOC, Workshop Report No. 98, p. 86.

Oguz, T., Aubrey, D., Latun, V., Demirov, E., Kolesnikov, L., Sur, H., Diaconu, V., Besiktepe, S., Duman, M., Limeburner, R., Eremeev, V., 1994. Mesoscale circulation and thermohaline structure of the Black Sea during HydroBlack '91. Deep-Sea Res. 41, 603–628.

Ovchinnikov, I.M., 1998. Interaction between surface and deep waters in the process of transverse circulation of the Black Sea. Ventilation of Black Sea Anoxic Waters. Workshop Rep. Ser., 1/05/98, pp. 135–161, Liege.

Ovchinnikov, I.M., Popov, Yu.I., 1987. Evolution of the cold intermediate layer in the Black Sea. Oceanology 27, 555–560.

Pacanowski, R.C., Dixon, K., Rosati, A., 1991. The GFDL Modular Ocean Model Users Guide, version 1.0. GFDL Ocean Group Tech. Rep., No 2, 176 pp.

Simeonov, J., Stanev, E., Backhaus, J., Jungclaus, J., Roussenov, V., 1997. Heat and salt intrusions in the picnocline from sinking plumes. Test case for the entrainment in the Black Sea. In: Ozsoy, E., Mikaelyan, A. (Eds.), Sensitivity to Change: Black Sea, Baltic Sea and North Sea. NATO ASI Series, vol. 27. Kluwer Academic Publishing, Dordrecht, The Netherlands, pp. 417–438.

Simonov, A.I., Altman, E.N. (Eds.), 1991. Hydrometeorology and Hydrochemistry of the USSR Seas. The Black Sea, vol. IV. Gidrometeoizdat, 430 pp.

Sorkina, A.I. (Ed.), 1974. Reference Book on the Black Sea Climate. Gidrometeoizdat, Moscow, 406 pp.

Speer, K., Tzipermann, E., 1992. Rates of water mass formation in the north Atlantic ocean. J. Phys. Oceaogr. 22, 93–104.

Stanev, E.V., 1990. On the mechanisms of the Black sea circulation. Earth-Sci. Rev. 28, 285–319.

Stanev, E.V., Staneva, J.V., 2000. The impact of the baroclinic eddies and basin oscillations on the transitions between different quasi-stable states of the Black Sea circulation. J. Mar. Sys. 24, 3–26.

Stanev, E.V., Staneva, J.V., 2001. The sensitivity of the heat exchange at ocean surface to meso and sub-basin scale eddies. Model study for the Black Sea. Dyn. Atmos. Oceans 33, 163–189.

Stanev, E.V., Staneva, J.V., Roussenov, V.M., 1997. On the Black Sea water mass formation. Model sensitivity study to atmospheric forcing and parameterization of some physical processes. J. Mar. Sys. 13, 245–272.

Stanev, E.V., Beckers, J.M., Lancelot, Ch., Staneva, J.V., Le Traon, P.Y., Peneva, E.L., Gregoire, M., 2002. Coastal-open ocean exchange in the Black Sea: observations and modeling. Submitted to Estuarine, Coastal Shelf Sci., in press.

Staneva, J.V., Stanev, E.V., 1997. Cold intermediate water mass formation in the Black Sea. Analyses on numerical model simulations. In: Özsoy, E., Mikaelyan, A. (Eds.), Sensitivity to Change: Black Sea, Baltic Sea and North Sea, NATO Series. Kluwer Academic Publishing, Dordrecht, The Netherlands, pp. 375–393.

Staneva, J.V., Stanev, E.V., 1998. Oceanic response to atmospheric forcing derived from different climatic data sets. Intercomparison study for the Black Sea. Oceanol. Acta 21, 393–417.

Staneva, J.V., Dietrich, D., Stanev, E., Bowman, M., 2001. Rim current and coastal eddy mechanisms in an eddy resolving Black Sea general circulation model. J. Mar. Sys. 31, 137–157.

Unluata, U., Oguz, T., Latif, M.A., Ozsoy, E., 1989. On the physical oceanography of the Turkish Straits. In: Pratt, G. (Ed.), The Physical Oceanography of Sea Straits. NATO ASI Ser., Ser. C. Kluver Academic, Norwell, MA, pp. 25–60.